Synthetic Metals 257 (2019) 116168

Contents lists available at ScienceDirect

Synthetic Metals

journal homepage: www.elsevier.com/locate/synmet

A negative effect of carbon phase on specific capacity of electrode material consisted of nanosized bismuth vanadate embedded in carbonaceous matrix

Andrzej P. Nowak[a,*], K. Trzciński[a], M. Szkoda[a], J. Karczewski[b], M. Gazda[b], A. Lisowska-Oleksiak[a]

[a] Faculty of Chemistry, Department of Chemistry and Technology of Functional Materials, Gdańsk University of Technology, Narutowicza 11/12, 80-233, Gdańsk, Poland
[b] Faculty of Applied Physics and Mathematics, Gdańsk University of Technology, Narutowicza 11/12, 80-233, Gdańsk, Poland

ARTICLE INFO

Keywords:
Negative electrode, Lithium-ion battery, Bismuth vanadate, Carbonaceus matrix

ABSTRACT

Lithium-ion batteries (LIBs) are widely used all over the world. The LIBs belong to a renewable energy source and energy storage devices. The increase in energy demand causes that new materials of higher energy and higher power densities are still under investigation. Herein, we compare electrochemical properties of bismuth vanadate ($BiVO_4$) embedded and not embedded into carbonaceous matrix as an anode material along with structural changes. Material incorporated into carbon phase ($BiVO_4$@C) exhibited much better electrochemical stability but with lower specific capacity (128 mA h/g) in comparison with pure $BiVO_4$ (217 mA h/g). XRD measurements showed the change in crystallographic structure due to lithium ion intercalation/extraction process. Hence, it seemed obvious that the presence of carbon affected the interfacial structural and electrochemical properties of bismuth vanadate based electrodes.

1. Introduction

Since first application of lithium-ion battery (LiBs) by SONY in 1991 there is a continuous increase in demand for such systems for energy storage and energy conversion. It is due to fact the we are surrounded by devices which can not work without battery system. In the beginning LiBs were used in small portable devices but recently they are found in electric vehicles. It is because lithium-ion batteries are environmental friendly and can offer high energy, long lifespan and low cost in comparison with nickel-cadmium (NiCd) and nickel-metal hydride (NiMH) batteries or supercapacitor systems [1,2]. However, recent progress of high-performance anode in large-scale applications forced graphite negative electrode in LiBs to be replaced. The theoretical capacity of graphite electrodes of 372 mA h/g is not attractive for such applications. Therefore many investigations regarding finding suitable negative electrode materials have been already undertaken. Such materials should exhibit higher specific capacity and improved rate capability. There are many kinds of electrode material which are expected to replace graphite *e.g.* polymer derived ceramics (PDCs) [3,4], transition metal oxides [5–7], non-graphitized hard carbons [8–10] or Li alloys [11,12]. Among them Li alloys are considered as one of the most promising materials. However, the Li alloy system suffers from volume changes, poor cycling performances due to pulverization leading to active material contact loss during the alloying and dealloying process [13]. To overcome these problems such electrode materials are modified with carbonaceous material. It is due to the fact that the carbon phase acts as a stress-acommodating phase [14–16].

Recently, bismuth vanadate ($BiVO_4$) was consider as an attractive anode material for lithium-ion batteries [17,18] or lithium ion capacitor [19] although this compound is known to be utilized in photocatalysis [20,21] or photoelectrocatalysis [22–24]. However, layered structure of $BiVO_4$ and the presence of bismuth and vanadium ions of different valencies makes this metal vanadate potential host for lithium ions insertion/extraction process as it is observed for reversible electrochemical conversion reaction of lithium with transition-metal compounds [25,26]:

$$M_aX_b + bnLi^+ + bne^- \leftrightarrows aM + bLi_nX \quad (1)$$

where M = transition metal *e.g.* Mn, Fe, Co, Ni, Cu *etc.*, X = anion (O, S, Se, F, N, P *etc.*).

The irreversible conversion reaction of $BiVO_4$ with Li^+ ions leads to formation of metallic Bi and Li_3VO_4:

$$BiVO_4 + 3Li^+ + 3e^- \leftrightarrows Bi + Li_3VO_4 \quad (2)$$

and further an alloy is formed:

$$Bi + 3Li^+ + 3e^- \leftrightarrows Li_3Bi \quad (3)$$

This kind of reactions is the main reason for excellent battery

* Corresponding author.
E-mail address: andnowak@pg.edu.pl (A.P. Nowak).

https://doi.org/10.1016/j.synthmet.2019.116168
Received 24 June 2019; Received in revised form 19 August 2019; Accepted 6 September 2019
Available online 30 September 2019

performance in any conversion reduction systems [27]. The theoretical capacity of a $BiVO_4$ based electrode material is 496 mA h/g and is higher than for the graphite electrode (372 mA h/g).

Moreover, $BiVO_4$ is known as an environmentally friendly yellow pigment that is widely used in a wide range of products such as ceramics and paints [28]. The very low toxicity of Bi and low manufacturing costs of $BiVO_4$ are advantageous in using bismuth vanadate as an electrode material.

In the present study we have investigated influence of carbonaceous matrix on electrochemical properties of negative electrode consisted of $BiVO_4$. Encapsulation of bismuth vanadate into carbon phase was expected to improve electric contact between particles and to enhance cyclability and rate capability as it was already observed for other inorganic-based negative electrode materials [29,30].

Materials were characterized with the solid-state physics techniques and finally, $BiVO_4$-based electrode was tested in half-cell configuration.

2. Experimental

Bismuth vanadate was prepared using the high temperature solid-state chemical reaction using equimolar amounts of $Bi(NO_3)_3{\cdot}5H_2O$ and NH_4VO_3. Grinded in mortar and pestle precursors were dried at 100 °C, pressed into a pellet (10 mm diameter) and annealed at 600 °C for 4 h. In order to prepare $BiVO_4$ incorporated in carbonaceous matrix ($BiVO_4$@C), two separate solutions of $BiVO_4$ precursors ($Bi(NO_3)_3{\cdot}5H_2O$ and NH_4VO_3) were prepared in 2 M HNO_3. Poly(ethylene oxide) (PEO) (M = 300,000, Aldrich) was added to the bismuth nitrate solution as a source of carbon. The subsequent viscous solution was mixed with NH_4VO_3 containing solution and stirred overnight. The molar ratio between Bi, V and C was equal to 1:1:1. Then, resulting slurry was dried at 120 °C followed by the annealing in Ar atmosphere at 600 °C for 4 h.

The Raman spectra were recorded using a confocal micro-Raman spectrometer (InVia, Renishaw) with sample excitation, by means of an argon ion laser emitting at 514 nm.

The phase composition of the samples was checked by an X-ray diffraction system in the range of $2\theta = 20 - 70^{\circ}$, using an X-ray diffractometer (Xpert PRO-MPD, Philips) with copper K_α radiation ($\lambda = 1.5404$ Å). The diffraction patterns were processed using Fityk software [31] *via* fitting to the Lorentzian function.

The morphology of the samples was investigated by the Schottky field emission scanning electron microscope (FEI Quanta FEG 250) with an ET secondary electron detector. The beam accelerating voltage was kept at 20 kV. For the purpose of elemental analysis, Energy Dispersive X-ray Spectroscopy was performed with the EDAX Genesis APEX 2i with the ApolloX SDD spectrometer, in particular areas of each sample.

An electrode film was prepared form a slurry containing $BiVO_4$ or $BiVO_4$@C, carbon black (CB) (Super P, Timcal, Switzerland) and pVDF (Polyvinylidene fluoride, Solvay) at weight ratio 7:2:1 dissolved in NMP (N-methyl-2-pyrrolidinone, AlfaAesar) on a copper current collector (Schlenk Metallfolien GmbH & Co KG, Germany). After tape casting material was dried, cut from the tape and pressed (60 s with a load of 100 MPa) followed drying under dynamic vacuum in an oven (Glass Oven B-585 Büchi, Germany) for 24 h at 90 °C. The mass of the electrode was ˜ 5 mg. Electrode material were tested in two-electrode Swagelok® cell with lithium foil (99.9%, 0.75 mm thickness, AlfaAesar) as counter and reference electrode. The SelectiLyte™ LP30 (1 M $LiPF_6$ in 1:1 wt/wt mixture of ethylene carbonate and diethyl carbonate) from Merck were used as electrolyte and glass fibre (Schleicher & Schüll, Germany) as the separator.

The battery tests of the samples were performed using the ATLAS 0961 MBI (Poland) multichannel battery testing system with different current densities from 0.01 V to 3 V. Cyclic voltammetry measurements (CV) were carried out on a PGSTAT302 N galvanostat/ potentiostat over the potential range from 0.005 V to 3 V *vs*. Li/Li^+ with a scanning rate of 0.1 mV/s.

The electrical conductivity of $BiVO_4$ and $BiVO_4$@C samples was performed by the two-terminal method. Pressed pellets of pure $BiVO_4$ and $BiVO_4$@C were immersed between stainless steel current collectors and a constant current was applied (Autolab PGSTAT10). Each pellet was prepared using SPECAC handpress (150 MPa load). The pellet diameter was 10 mm and the thickness was in the range between 0.5 and 0.7 mm.

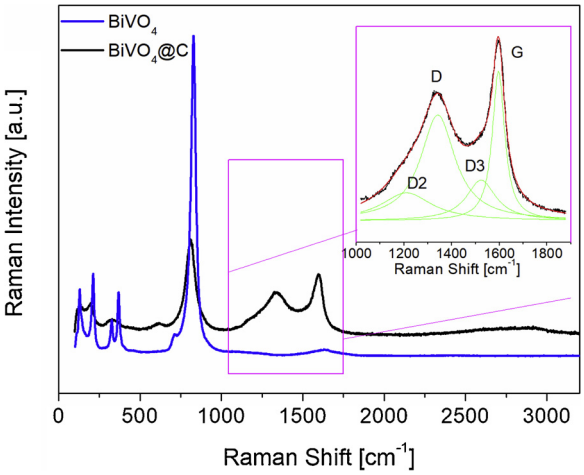

Fig. 1. Raman spectra for $BiVO_4$ (——) and $BiVO_4$@C (——) electrode materials. Inset: Curve fit for the first order Raman spectra of $BiVO_4$@C.

3. Results and discussion

The Raman spectra of pure $BiVO_4$ powder and $BiVO_4$@C powder are presented in Fig. 1. The common feature of both materials is the presence of maxima in the range 100 – 1000 cm^{-1}. The characteristic peaks for pure $BiVO_4$ are seen at 130 cm^{-1}, 211 cm^{-1}, 326 cm^{-1}, 368 cm^{-1}, 713 cm^{-1} and 828 cm^{-1}. The first two Raman bands origin from lattice modes [32,33]. The Raman bands at 326 cm^{-1} and 368 cm^{-1} are attributed to the asymmetric and symmetric stretching mode of VO_4 tetrahedron [34] while stretching modes of two vibrational modes of V—O are detected at 713 cm^{-1} and 828 cm^{-1} [35]. However, Raman modes of pure $BiVO_4$ powder and $BiVO_4$@C do not overlap. For $BiVO_4$@C Raman bands at around 130 cm^{-1}, 199 cm^{-1} and 811 cm^{-1} as well as broad humps at 330 cm^{-1} and 613 cm^{-1} were seen. It is known that position of vibrational mode of V—O is possible to be shifted due to different factors *e.g.* the calcination temperature [34] and this shift is related to the bond distance between vanadium and oxygen [35]. Thus, we assumed that the presence of cabonaceous matrix affected the crystallographic structure of $BiVO_4$ and influenced on the V—O bond length.

The main difference in Raman spectrum between both materials is seen in the range 1000–2000 cm^{-1}. This region is known to be characteristic for carbonaceous materials *e.g.* graphite and disordered carbons. In Fig. 1, one may see two peaks, the D peak around 1350 cm^{-1} and the G peak around 1580–1600 cm^{-1} [36]. Both maxima are attributed to the presence of carbon atoms of sp^2 hybridization. The D peak origins from the breathing motion of sp^2-ring, while the G maximum is attributed to an in-plane bond stretching vibrations of sp^2 carbon atoms [37].

In the literature one may find that one should apply fitting procedure in the interpretation Raman spectra of disordered carbonaceous materials [38,39]. In the inset in Fig. 1 curve fit for first-order Raman spectra is shown (for more details see Table S1). The D and D2 bands are attributed to the presence of disordered graphitic lattice while the D3 band confirms the presence of amorphous carbon phase. The G band is characteristic for ideal graphitic lattice. Direct relation between D and G peaks intensities allows to estimate cluster size of the graphitic microcrystals, known as L_a parameter (in-plane correlation length)

Table 1
Raman peak positions and assignment of major vibrational bands of $BiVO_4$ and $BiVO_4$@C electrode materials.

Raman Shift [cm^{-1}]	Band
130	Lattice modes in $BiVO_4$
211	Lattice modes in $BiVO_4$
326	Asymmetric stretching mode of VO_4
368	Symmetric stretching mode of VO_4
713	Stretching vibrations of V-O
828	Stretching vibrations of V-O
~ 1350	Breathing motion of sp^2-ring (C-C)
~ 1590	Stretching vibrations of (C-C)

Carbon cluster size L_a = 6.3 nm.

[40]:

$$\frac{I(D)}{I(G)} = \frac{C(\lambda)}{L_a} \quad (4)$$

were C = 44 Å (for the Raman laser excitation energy λ = 514.5 nm).

This formula can be applied assuming that there were no direct interactions between carbon and any metal form $BiVO_4$. The calculated L_a parameter is equal to 6.3 nm which is higher in comparison with the graphite powder (4.2 nm) and is lower in comparison with highly oriented pyrolytic graphite (HOPG) (> 17 nm) [41]. The low L_a value suggests that carbon is less ordered in the studied case.

The summarized data data for Raman Spectroscopy is given in Table 1.

The XRD pattern of $BiVO_4$ and $BiVO_4$@C before and after galvanostatic cycles are shown in Fig. 2. One may see that XRD pattern of both materials are identical and suggest the formation of monoclinic crystals, with space group I112/b [42], z = 4, and cell parameters a = 7.247 Å, b = 5.096 Å, c = 11.702 Å and γ = 134.18°. This structure shows eight-fold oxygen coordination of Bi atom forming distorted Bi-O dodecahedron (BiO_8) with twelve faces. The oxygen atoms take part also in four-fold coordination around V atoms and form regular VO_4 tetrahedron. Such structure forms layer-like system which might be suitable for lithium ion insertion/extraction process that is observed in layered cathode materials *i.e.* $LiCoO_2$, $LiNi_{1/3}Mn_{1.3}O_{1/3}$ [43]. In Fig. 2b one may see that after galvanostatic cycles $BiVO_4$ and $BiVO_4$@C active materials exhibited different crystallographic structure in comparison with material before electrochemical cycles. On the one hand, one may see that lithium insertion and extraction process might cause decomposition of bismuth (III) vanadate with formation of bismuth and vanadium metal oxides of different stoichiometry (see, Fig. 2b). On the other hand it is confirmed that LiF and Li_2CO_3 were identified. Lithium

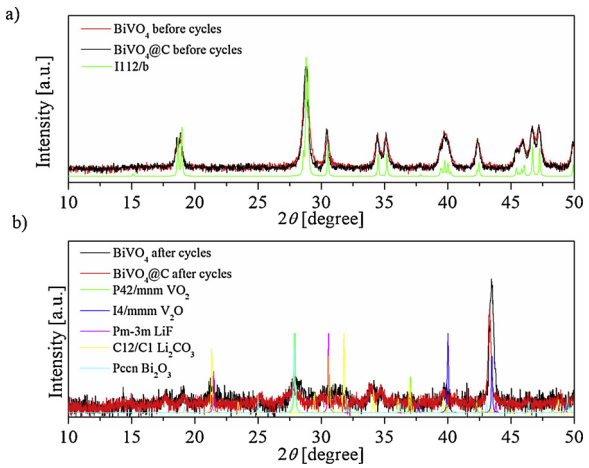

Fig. 2. XRD pattern of $BiVO_4$ and $BiVO_4$@C electrodes before (a) and after (b) galvanostatic cycles.

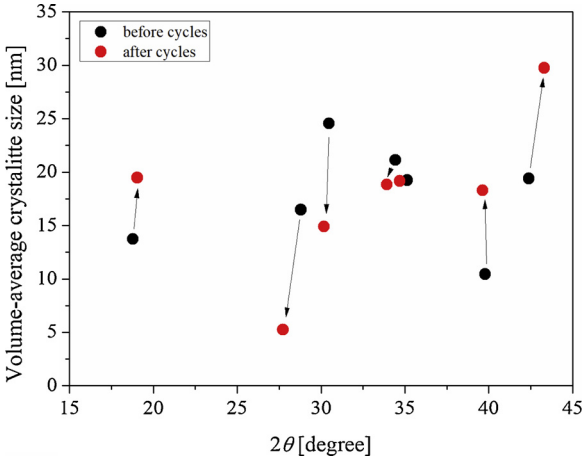

Fig. 3. Changes in dimension of volume-average crystallite size before and after electrochemical charging/discharging processes of $BiVO_4$@C electrode material.

compounds are known to form solid electrolyte interphase (SEI) which is formed due to electrolyte decomposition during cycling [44]. Position of maxima attributed to SEI film compounds might overlap with the position of $BiVO_4$. We did not observed formation of metallic Bi nor Li_3VO_4.

The volume-average crystallite size (D_{ap}), calculated from Scherrer equation [45], is 16 nm and 5 nm for material before and after electrochemical testing, respectively. The change in particle size evidenced that lithium insertion into $BiVO_4$ structure caused changes in its crystallographic lattice.

Fig. 3 shows changes in diameter of D_{ap} in the 2θ region from 15° to 45°.

It is very likely that shifts in peak maxima position as well as differences in the D_{ap} were due to lithium ion insertion and extraction process. We suppose that several factors might contributed to the observed phenomenon *e.g.* grain surface relaxation, non-uniform lattice distortions, inhomogeneity of the material.

SEM images of $BiVO_4$ and $BiVO_4$@C electrode materials are shown in Fig. 4.

Pure $BiVO_4$ material exhibited a cuboid structure of the particle of the size in nano scale ranging from 80 nm to over 700 nm (Fig. 4a). For $BiVO_4$@C material one may see that bismuth vanadate particles are embedded into carbonaceous matrix (See Fig. 1S). Their size is below 150 nm suggesting that $BiVO_4$ underwent morphological changes during modification with PEO followed thermal treatment. According to the SEM micrographs presented in Fig. S2, material prepared *via* annealing in a presence of PEO is not perfectly homogeneous. Rarely, the round-shaped particles with varied diameters uncovered with carbonaceous phase were detected. EDX analysis shows that the Bi:V ratio is disturbed due to the excess of Bi. The annealing process of $BiVO_4$/PEO mixture performed in Ar atmosphere at 600 °C lead to the formation of carbon phase and simultaneously may lead to the partial reduction of Bi^{3+} to Bi^0 [46]. However, no reflexes from metallic bismuth were recorded in XRD pattern.

Moreover, carbonaceous matrix seemed to be porous and of amorphous origin. One may notice that average size of $BiVO_4$ of both materials were of one order of magnitude higher in comparison with the results obtained from Scherrer equation. This may evidenced that bismuth vanadate crystallites form an agglomerated structures seen on SEM. It is very likely that the carbon phase partially prevented adverse agglomeration as the size of particles of $BiVO_4$@C was lower in comparison with particle size of bare $BiVO_4$.

The cyclic voltammetry curves of $BiVO_4$ and $BiVO_4$@C electrodes are presented in Fig. 5a and b, respectively. In the first reduction scan one may see three cathodic maxima at ~ 1.75 V, ~ 1.0 V and ~ 0.56 V for

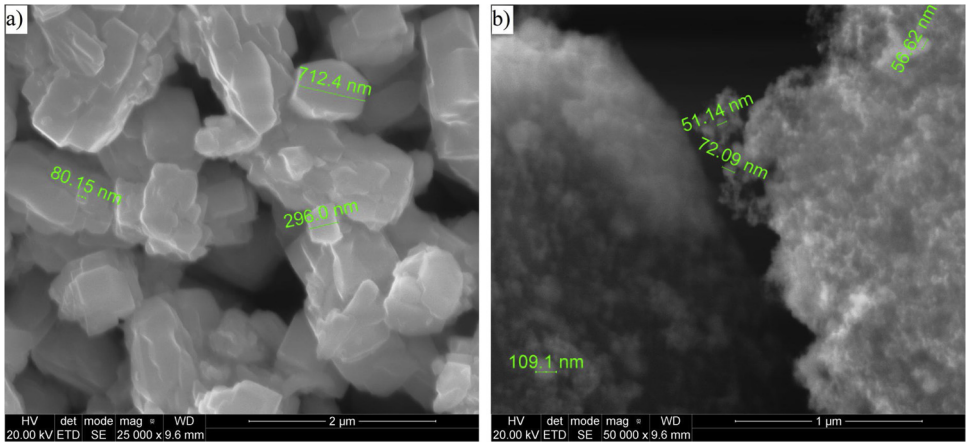

Fig. 4. The SEM image of a) $BiVO_4$ and b) $BiVO_4$@C electrode materials.

$BiVO_4$, and ˜ 1.75 V, ˜ 1.31 V and ˜ 0.5 V for $BiVO_4$@C, respectively. It is very likely that the maximum at ˜ 1.75 V for both materials is attributed to metallic bismuth formation as it was observed for bismuth oxide [47]. One may see a noticeable difference in peak intensity of the cathodic current maxima between both electrode materials at 1.75 V. This difference is due to presence or lack of carbonaceous matrix for $BiVO_4$ and $BiVO_4$@C, respectively. It is very likely that carbon phase acts as a layer which in some way prevents $BiVO_4$ decomposition with formation of metallic bismuth. We suppose that in studied case the carbonaceous matrix does not form sufficient pathway for reaction between lithium and bismuth (III) vanadate. Thus, one may see that current density is lower for $BiVO_4$@C in comparison with current density recorded for $BiVO_4$. The mechanism of reaction with lithium might be as follow:

$$BiVO_4 + xLi^+ + xe^- \leftrightarrows \frac{x}{3}Bi + Li_xBi_{1-\frac{x}{3}}VO_4 \quad (5)$$

The cathodic peak maxima at ˜ 1.0 V for $BiVO_4$ and at ˜ 1.31 V $BiVO_4$@C is very likely to lead to Li_3VO_4 formation according to reaction:

$$Li_xBi_{1-\frac{x}{3}}VO_4 + (3-x)Li^+ + (3-x)e^- \leftrightarrows (1-\frac{x}{3})Bi + Li_3VO_4 \text{ for } 0 < x < 3 \quad (6)$$

The difference in a peak position might be originating from the fact that in case of $BiVO_4$@C the inorganic component is embedded in carbonaceous matrix. It may shift reduction reaction maximum towards higher potentials as additional resistance originating from the carbon phase occurred, according to Ohm's law. The origin of the third reduction maximum, at ˜ 0.56 V for $BiVO_4$ and at ˜ 0.5 V for $BiVO_4$@C, is complex. It might be attributed to both V^{5+} reduction to V^{4+} on the one hand [48], and to Li_3Bi formation, on the other hand [19]. In the subsequent cycles each of these maxima are split into two cathodic maxima the first at ˜ 0.52 V and the second at ˜ 0.72 V. The former origins from the reduction of V^{4+} to V^{3+}, and the latter is attributed to Li_3Bi alloy formation [25,49].

During anodic process one may see sharp anodic maximum at ˜ 1.0 V. It seems that the discharging leads to $BiVO_4$ formation during conversion and dealloying according to reaction:

$$Li_3Bi + Li_3VO_4 \leftrightarrows BiVO_4 + 6Li^+ + 6e^- \quad (7)$$

However, the reaction mentioned above is not 100% efficient as an another anodic maximum is seen at ˜ 1.2 V for $BiVO_4$ electrode material. This activity might be attributed to some oxidation process of V^{3+} to V^{5+} [[[25]]]. This process is not recorded for $BiVO_4$@C. It suggests that the presence of carbonaceous matrix affects some redox couple activities, very likely of pseudocapacitive character. The anodic maxima at ˜ 2.6 V for $BiVO_4$ and 2.7 V for $BiVO_4$@C, correspond to oxidation of metallic Bi [[[25]]].

In Fig. 6 galvanostatic charge/discharge curves of $BiVO_4$ and $BiVO_4$@C electrodes for the first three cycles in half cell configuration performed in the potential range from 0.05 V to 2.5 V at current density $j = 40$ mA/g.

One may see that curve plateau observed in the first charge/discharge overlaps with cathodic/anodic current maxima seen in cv plot (see Fig. 5). It is shown that the presence of carbonaceous matrix affects electrochemical properties of $BiVO_4$@C electrode material. However, this was not a positive effect as the specific capacity of $BiVO_4$@C electrode material was lower in comparison with $BiVO_4$ electrode material. In both cases one may see significant capacity loss during first lithium insertion process. This capacity loss might be related with solid electrolyte interphase (SEI) formation [[25]] as well as with irreversible reaction of BiO_x with lithium oxide formation:

$$BiO_x + xLi^+ + xe^- \leftrightarrows Bi + Li_xO \quad (8)$$

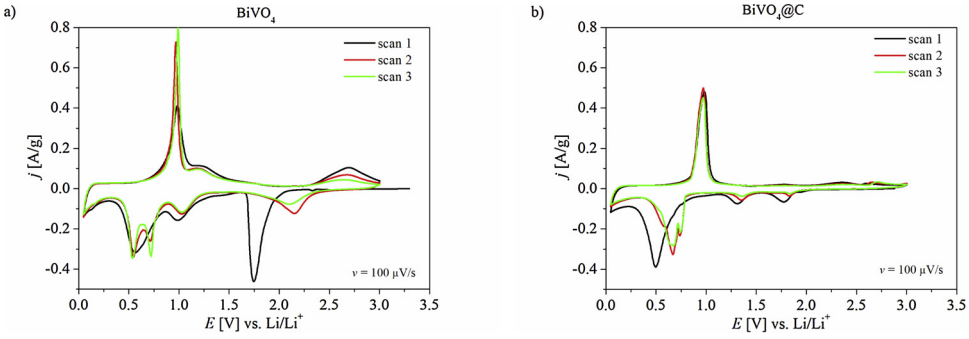

Fig. 5. The cyclic voltammetry curves of the a) $BiVO_4$ and b) $BiVO_4$@C in LP30 electrolyte.

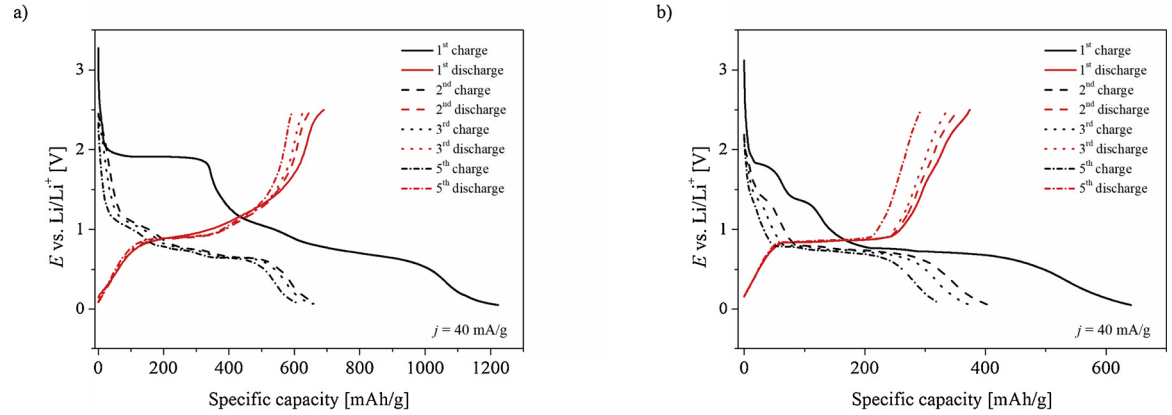

Fig. 6. The galvanostatic charge/discharge curves of a) $BiVO_4$ and b) $BiVO_4$@C in LP30.

According to Gomez-Romero et al. the overall reaction between Li^+ and $BiVO_4$ is as follow:

$$BiVO_4 + 6Li^+ + 6e^- \leftrightarrows Li_3Bi + Li_3VO_4 \quad (9)$$

and gives the theoretical capacity of 662 mA h/g [21].

However, taking into account the molar mass of $BiVO_4$ (323.92 g/mol), Faraday's 1st law of electrochemistry (1 g equivalent weight of a material will deliver 96,485 coulombs (or 26,801 mA h)) and taking into account 6 electrons one may calculate theoretical capacity:

$$Q = \frac{26801 \cdot 6}{323.92} = 496\ [mAh/g] \quad (10)$$

And even though the theoretical capacity is not 662 mA h/g but 496 mA h/g it is still over 100 mA h/g higher than for graphite anode (Q_{th} = 372 mA h/g).

In the studied case first charge/discharge capacities are 1223 mA h/g and 690 mA h/g for $BiVO_4$, and 641 mA h/g and 373 mA h/g for $BiVO_4$@C. Such high values origins from SEI formation during first process of lithium ions incorporation into a negative electrode materials [50]. These values are diminishing with subsequence cycles and after fifth cycle gave specific discharge capacities of 594 mA h/g and 293 mA h/g for $BiVO_4$ and $BiVO_4$@C, respectively. The capacity retention after 5 cycles at j = 40 mA/g was equal to 86% for $BiVO_4$ and 78% for $BiVO_4$@C. The relationship between cycle number and current rate is given in Fig. 7.

One may see that for $BiVO_4$ electrode material there is continuous decrease of capacity value with cycle number. It is very likely due to fact that no stable phase of $BiVO_4$ were formed, yet. It may be also caused by the continuous SEI formation and growth leading to capacity fading. In the present study the final discharge capacity was equal to 217 mA h/g for current density of 40 mA/g. Contrary, the $BiVO_4$@C negative electrode exhibited almost straight horizontal line suggesting, that after first several charging/discharging cycles electrode material formed stable phase. The presence of carbon matrix might influenced the SEI formation followed the formation of the stable phase of $BiVO_4$. The SEI is known to prevent further reduction of the electrolyte and to ensure electrochemical stability of an electrode. Synergistic effect due to the SEI formation and the presence of carbonaceous matrix improved the stability of the $BiVO_4$@C electrode material during charging/discharging. However, this stability had negative effect on the capacity of such electrode. The discharge capacity of the last discharge capacity was only 128 mA h/g. We assumed that electrode material consisted of $BiVO_4$ embedded into carbonaceous matrix ($BiVO_4$@C) would be more stable during subsequent cycles with retained capacity originating from $BiVO_4$ with improved electrical conductivity. The calculated electrical conductivities for pure $BiVO_4$ and $BiVO_4$@C were $1 \cdot 10^{-10}$ S/cm and $2 \cdot 10^{-2}$ S/cm, respectively. In the literature one may found that the electric conductivity of pure $BiVO_4$ is ~ $1 \cdot 10^{-9}$ S/cm for 625 K [51] and according to Arrhenius equation it decreases with temperature increase. However, it turned out that $BiVO_4$@C electrode material exhibited worse electrochemical performances in comparison with $BiVO_4$ without carbonaceous matrix. It suggests that the type of carbon phase plays important role in electrochemical behaviour of electrode material with carbonaceous matrix expected to act as material improving electric contact between electrode active material particles and enhancing their cyclability and rate capability. Recently, Majchrzycki et al. showed that for non-reduced graphene oxide the capacity of such electrode material was lower in comparison with photothermally reduced GO [52]. It confirms that the type of carbon phase affects the electrochemical performance of an electrode material. It is very likely that in the studied case the source of carbon was not suitable chosen to improve electrode performance of the whole electrode material.

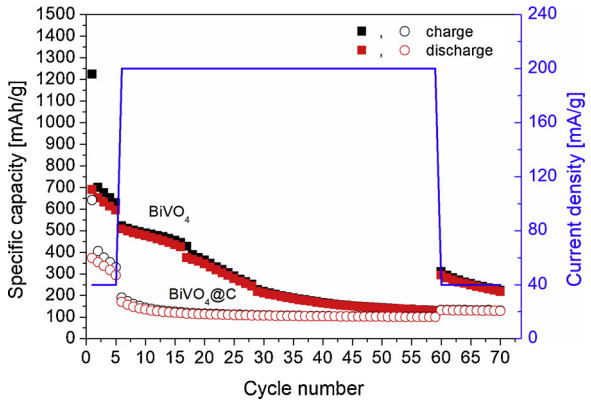

Fig. 7. Relationship between specific capacity and the number of cycles.

4. Conclusion

Two kind of electrode material consisted of $BiVO_4$ were prepared, characterized and compared for their usage in lithium-ion battery application. It was evidenced that both pure $BiVO_4$ and $BiVO_4$ embedded into carbonaceous matrix ($BiVO_4$@C) exhibited identical crystallographic structure, however SEM images showed that morphology of the material was affected. The structure underwent structural changes due to lithium ion insertion/extraction seen as a change of the volume-average crystallite size of the electrode material. Electrochemical tests evidenced that $BIVO_4$ is suitable for lithium ion intercalation/extraction process. The $BiVO_4$@C electrode material exhibited improved cyclability but suffered from low capacity in comparison with pure $BiVO_4$. The capacities of 217 mA h/g for $BiVO_4$ and 128 mA h/g for $BiVO_4$@C are not an alternative for replacement of graphite electrode at the moment. Nevertheless, improvement of capacity of $BiVO_4$@C seems to

be a crucial issue to be able to utilize such material for lithium-ion batteries.

Acknowledgement

This work was supported by the Polish Ministry of Science and Higher Education (DS no. 032406 and Mini Grant No. 4914/E-359/M/2018)

Appendix A. Supplementary data

Supplementary material related to this article can be found, in the online version, at doi:https://doi.org/10.1016/j.synthmet.2019.116168.

References

[1] M. Szkoda, K. Trzciński, J. Rysz, M. Gazda, K. Siuzdak, A. Lisowska-Oleksiak, Solid State Ion. 302 (2017) 197–201.
[2] J. Libich, J. Máca, J. Vondrák, O. Čech, M. Sedlaříková, J. Energy Storage 17 (2018) 224–227.
[3] M. Wilamowska-Zawlocka, P. Puczkarski, Z. Grabowska, J. Kaspar, M. Graczyk-Zajac, R. Riedel, G.D. Soraru, RSC Adv. 106 (2016) 104597–104607.
[4] Y. Feng, S. Dou, Y. Wei, Y. Zhang, X. Song, X. Li, V.S. Battaglia, ACS Omega 11 (2017) 8075–8085.
[5] K. Cao, T. Jin, L. Yang, L. Jiao, Mater. Chem. Front. 1 (2017) 2213–2242.
[6] A. Chojnacka, M. Molenda, M. Bakierska, R. Dziembaj, ESC Trans. 64 (2015) 165–171.
[7] Y.-C. Kuo, H.-T. Peng, Y. Xiao, J.-Y. Lin, J. Solid State Electrochem. 20 (2016) 1625–1631.
[8] W. Li, M. Chen, C. Wang, Mater. Lett. 65 (2011) 3368–3370.
[9] M. Bakierska, M. Molenda, D. Majda, R. Dziembaj, Procedia Eng. 98 (2014) 14–19.
[10] P.-Y. Zhao, J.-J. Tang, C.-Y. Wang, J. Solid State Electrochem. 21 (2017) 555–562.
[11] Q. Sun, B. Zhang, Z.-W. Fu, Appl. Surf. Sci. 254 (2008) 3774–3779.
[12] G. Wang, X. Xiong, Z. Lin, C. Yang, Z. Lin, M. Liu, Electrochim. Acta 242 (2017) 159–164.
[13] J.W. Choi, D. Aurbach, Nat. Rev. Mater. 1 (1-16) (2016) 16013.
[14] R. Hu, W. Sun, M. Zeng, M. Zhu, J. Energy Chem. 23 (2014) 338–345.
[15] A. Chojnacka, M. Świętosławski, W. Maziarz, R. Dziembaj, M. Molenda, Electrochim. Acta 209 (2016) 7–16.
[16] J. Yang, L. Xi, J. Tang, F. Chen, L. Wu, X. Zhou, Electrochim. Acta 217 (2016) 274–282.
[17] D.P. Dubal, D.R. Patil, S.S. Patil, N.R. Munirathnam, P. Gomez-Romero, ChemSusChem 10 (21) (2017) 4163–4169.
[18] A. Ruud, J. Sottmann, P. Vajeeston, H. Fjellvåg, Phys. Chem. Chem. Phys. 20 (2018) 29798–29803.
[19] D.P. Dubal, K. Jayaramulu, R. Zboril, R.A. Fischer, P. Gomez-Romero, J. Mater. Chem. A 6 (2018) 6096–6106.
[20] L. Xu, Y. Wei, W. Guo, Y. Guo, Y. Guo, Appl. Surf. Sci. 332 (2015) 682–693.
[21] K. Trzciński, M. Szkoda, M. Sawczak, J. Karczewski, A. Lisowska-Oleksiak, Appl. Surf. Sci. 385 (2016) 199–208.
[22] K. Trzciński, M. Szkoda, K. Siuzdak, M. Sawczak, A. Lisowska-Oleksiak, Electrochim. Acta 222 (2016) 421–428.
[23] Y. Wang, N. Lu, M. Luo, L. Fan, K. Zhao, J. Qu, J. Guan, X. Yuan, Appl. Surf. Sci. 463 (2019) 234–243.
[24] J. Li, L. Guo, N. Lei, Q. Song, Z. Liang, ChemElectroChem 4 (2017) 2852–2861.
[25] M.R. Palacin, Chem. Soc. Rev. 38 (2009) 2565–2575.
[26] Y. Lu, L. Yu, X.W. Lou, Chemistry 4 (2018) 972–996.
[27] J. Sottmann, M. Herrmann, P. Vajeeston, A. Ruud, C. Drathen, H. Emerich, D.S. Wragg, H. Fjellvåg, Chem. Mater. 29 (2017) 2803–2810.
[28] Wendusu, T. honda, T. Masui, N. Imanaka, RSC Adv. 3 (2013) 24941–24945.
[29] J. Luo, X. Zhao, J. Wu, H.D. Jang, H.H. Kung, J. Huang, J. Phys. Chem. Lett. 3 (2012) 1824–1829.
[30] Y.H. Xu, Q. Liu, Y.J. Zhu, Y.H. Liu, A. Langrock, M.R. Zachariah, C.S. Wang, Nano Lett. 13 (2013) 470–474.
[31] M. Wojdyr, J. Appl. Cryst. 43 (2010) 1126–1128.
[32] R.L. Frost, D.A. Henry, M.L. Weier, W. Martens, J. Raman Spectrosc. 37 (2006) 722–732.
[33] D. Zhou, L.-X. Pang, W.-G. Qu, C.A. Randall, J. Guo, Z.-M. Qi, T. Shao, X. Yao, RSC Adv. 3 (2013) 5009–5014.
[34] S.R.M. Thalluri, C. Martinez-Suarez, A. Virga, N. Russo, G. Sarcacco, Int. J. Chem. Eng. Appl. 4 (2013) 305–309.
[35] F.D. Hardcastle, I.E. Wachs, J. Phys. Chem. 95 (1991) 5031–5041.
[36] F. Tuinstra, J.I. Koenig, J. Chem. Phys. 53 (1970) 1126–1130.
[37] M. Marcinek, L.J. Hardwick, G.Z. Żukowska, R. Kostecki, Carbon 48 (2010) 1552–1557.
[38] A. Sadezky, H. Muckenhuber, H. Grothe, R. Niessner, U. Pöschl, Carbon 43 (2005) 1731–1742.
[39] A.P. Nowak, B. Wicikowska, A. Lisowska-Oleksiak, Solid State Ion. 263 (2014) 131–139.
[40] A.C. Ferrari, J. Robertson, Physial Rev. B 61 (2000) 14095–14107.
[41] Y. Wang, D.C. Alsmeyer, R.L. McCreery, Chem. Mater. 2 (1990) 557–563.
[42] J.-C. Liu, J.-P. Chen, D.-Y. Li, Acta Phys. Sin.-Chem. Ed. 32 (1983) 1053–1060.
[43] C. Julien, A. Mauger, K. Zaghib, H. Groult, Materials 9 (2016) 595–620.
[44] S. Chattopadhyay, A.L. Lipson, H.J. Karmel, J.D. Emery, T.T. Fister, P.A. Fenter, M.C. Hersam, M.J. Bedzyk, Chem. Mater. 24 (2012) 3038–3043.
[45] P. Scherrer, Nachr. Ges. Wiss. Göttingen 26 (1918) 98–100.
[46] W. Cui, F. Wang, J. Wang, H. Liu, C. Wang, Y. Xia, J. Power Sources 196 (2011) 3633–3639.
[47] Y. Li, M.A. Trujillo, E. Fu, B. Patterson, L. Fei, Y. Xu, S. Deng, S. Smirnov, H. Luo, J. Mater. Chem. A 1 (2013) 12123–12127.
[48] L.L. Zhou, S.Y. Shen, X. Peng, L.N. Wu, Q. Wang, C.H. Shen, T.T. Tu, L. Huang, J.T. Li, S.G. Sun, ACS Appl. Mater. Interfaces 8 (2016) 23739–23745.
[49] D. Bresser, S. Passerini, B. Scrosati, Energy Environ. Sci. 9 (2016) 3348–3367.
[50] A. Wang, S. Kadam, H. Li, S. Shi, Y. Qi, NPJ Comput. Mater. 4 (1-26) (2018) 15.
[51] M. Hartmanova, M.T. Le, M. Jergel, V. Smatko, F. Kundracik, Russ. J. Electrochem. 45 (2009) 621–629.
[52] Ł. Majchrzycki, M. Walkowiak, A. Martyła, M.Y. Yablokov, M. Nowicki, R. Czajka, Mater. Sci.-Poland 34 (2016) 481–486.